PCCP

PAPER

View Article Online
View Journal | View Issue

Cite this: *Phys. Chem. Chem. Phys.*, 2026, **28**, 1963

SIFT-MS analysis of amines: unusually efficient O_2 addition to the radical cation product

Christoph Schaefer, *[a] Kseniya Dryahina, [a] Patrik Španěl, [a] Mark J. Perkins[b] and Vaughan S. Langford [c]

Selected ion flow tube mass spectrometry (SIFT-MS) is routinely used for real-time detection of volatile organic compounds (VOCs), including amines that are relevant in pharmaceutical, environmental, and food safety applications. As VOC monitoring in SIFT-MS depends on the knowledge of the underlying ion–molecule reactions, a comprehensive understanding of the ionisation processes is key for robust analyte identification and accurate quantitation. This study investigates the product ion formation of selected primary and secondary amines with H_3O^+, NO^+ and $O_2^{+\bullet}$ reagent ions. All reactions proceed at or near the collisional limit. While proton transfer from H_3O^+ yields the intact protonated molecule, charge transfer from $O_2^{+\bullet}$ predominantly leads to fragment ions. Notably, NO^+ reactions with all investigated amines yield an unusual product ion at nominal mass + 32, with its observed product ion ratio exhibiting substantial differences between compounds. The experimental data indicate an equilibrium reaction, initially suggestive of adduct formation between the radical cations and O_2. However, quantum chemical modelling shows that simple van der Waals adducts are thermodynamically unstable at the instrument temperature (393 K). Instead, the results support a reaction mechanism in which the nascent radical cation undergoes an intramolecular hydrogen shift to form a distonic ion that subsequently binds O_2. This pathway is exergonic for all four amines studied, and the computed Gibbs energy changes agree closely with values derived from observed experimental equilibrium constants under quasi-steady-state conditions, explaining the observed differences in product ion ratios. These results provide more detailed mechanistic insights into the O_2 addition of amine radical cations.

Received 16th October 2025,
Accepted 18th December 2025

DOI: 10.1039/d5cp03987h

rsc.li/pccp

Introduction

Detection and monitoring of amines is critical in several pharmaceutical and environmental applications due to their wide occurrence and potential health implications. In pharmaceutical manufacturing, amine impurities can arise from synthetic intermediates and reagents.[1] Secondary and tertiary amines can undergo nitrosation reactions with nitrous acid or other nitrosating agents to form *N*-nitrosamines.[1–3] Many *N*-nitrosamines have been shown to be genotoxic in animal studies, and several are classified by the International Agency for Research on Cancer (IARC) as probable or possible human carcinogens and therefore the International Council for Harmonisation (ICH) guidance designates these as ''cohort of concern''.[1,4–6] Their discovery in pharmaceutical products has triggered product recalls and new regulatory guidance, including reassessment of synthesis routes and controls.[3] Accurate identification and quantification of amines are therefore essential to ensure product safety.

Beyond pharmaceuticals, amines are also important in environmental and food quality monitoring. Many volatile amines are odorous volatile organic compounds (VOCs), contributing to air pollution and nuisance odours. Furthermore, in post combustion CO_2-capture systems, amines are widely used for chemical absorption to remove CO_2 and can therefore be emitted through the cleaned exhaust gas, necessitating environmental monitoring.[7,8] In food, biogenic amines are formed *via* decarboxylation of amino acids or transamination of ketones and aldehydes.[9,10] Elevated levels can indicate spoilage, microbial contamination, or degradation, thereby serving as valuable indicators for freshness and safety.[11,12] At sufficient doses, several biogenic amines can cause adverse health effects.[13,14]

To address these needs, different chromatographic techniques have been developed. Gas chromatography (GC)[11,15,16] offers high sensitivity for volatile amines, whereas liquid chromatography (LC) is preferred for non-volatile and polar amines and is routinely used in environmental[17] or pharmaceutical analysis.[18,19] However, in GC analysis, amines often exhibit peak tailing or loss due to adsorption on active sites within the

[a] *J. Heyrovský Institute of Physical Chemistry of the Czech Academy of Sciences, Dolejškova 3, 18223 Prague 8, Czech Republic*
[b] *Da Vinci Laboratory Solutions UK & Ireland Limited, Cambridge CB3 0NA, UK*
[c] *Syft Technologies Limited, Christchurch 8011, New Zealand*

inlet or column, often requiring derivatisation.[20] In addition, many conventional chromatographic methods require additional sample preparation steps, are time-consuming, and do not provide real-time data. To overcome these limitations, selected ion flow tube mass spectrometry SIFT-MS has emerged as a robust and versatile technique for monitoring VOCs.[21,22] SIFT-MS enables direct, real-time, and quantitative VOC analysis at trace levels without requiring complex sample preparation. In SIFT-MS, mass-selected reagent ions react with neutral compounds in a flow tube under controlled conditions. The known product ion formation mechanisms (*i.e.*, product branching ratios and reaction rate coefficients) enable accurate VOC quantitation. The ion–molecule reactions initiated by the positive reagent ions H_3O^+, NO^+ and $O_2^{+\bullet}$ under SIFT conditions are typically well understood.[23] For sufficiently exothermic reactions, H_3O^+ usually transfers a proton to yield the protonated molecule MH^+ as depicted in reaction (1).

$$H_3O^+ + M \rightarrow MH^+ + H_2O \quad (1)$$

With NO^+, often charge transfer generates the radical cation $M^{+\bullet}$ (reaction (2)), although alternative channels such as hydride ion transfer (reaction (3)), producing $(M - H)^+$, or adduct formation (reaction (4)), producing $(M{\cdot}NO)^+$, are also possible.

$$NO^+ + M \rightarrow M^{+\bullet} + NO^\bullet \quad (2)$$

$$NO^+ + M \rightarrow (M - H)^+ + HNO \quad (3)$$

$$NO^+ + M \rightarrow (M{\cdot}NO)^+ \quad (4)$$

$O_2^{+\bullet}$ typically ionizes molecules *via* charge transfer as well as depicted in reaction (5), but the high ionisation energy of O_2 often results in dissociative charge transfer, producing fragment ions (reaction (6) or (7)).

$$O_2^{+\bullet} + M \rightarrow M^{+\bullet} + O_2 \quad (5)$$

$$O_2^{+\bullet} + M \rightarrow [M - R]^{+\bullet} + R + O_2 \quad (6)$$

$$O_2^{+\bullet} + M \rightarrow [M - R]^{+\bullet} + R^\bullet + O_2 \quad (7)$$

Gas-phase amine radical cations display distinctive behaviour. Initially, both the positive charge and the radical site reside on nitrogen, but intramolecular hydrogen shifts can generate distonic ions in which the charge remains on nitrogen but the radical site is relocated to a carbon atom (reaction (8)).[24,25] These distonic ions may revert to the conventional radical cation,[26,27] fragment to NH_4^+ or alkyl cations (reaction (9) or (10)), rearrange nitrogen-containing groups between carbon atoms,[27] or undergo O_2 addition at the carbon-centred radical site (reaction (11)).[28,29]

$$M^{+\bullet} \rightleftharpoons M_{dist}^{+\bullet} \quad (8)$$

$$M_{dist}^{+\bullet} \rightarrow [M - R]^{+\bullet} + R \quad (9)$$

$$M_{dist}^{+\bullet} \rightarrow [M - R]^{+} + R^\bullet \quad (10)$$

$$M_{dist}^{+\bullet} + O_2 \rightleftharpoons (M + O_2)^{+\bullet} \quad (11)$$

As ground-state O_2 is itself a triplet diradical, it can readily couple with the carbon-centered radical site of such a distonic ion, facilitating adduct formation. Such O_2 addition is not unique to amines and has been reported for other distonic cations as well.[30–33] The intramolecular hydrogen shift from the conventional radical cation to the corresponding distonic radical cation proceeds entirely on the doublet potential energy surface and does not involve any change in spin multiplicity. In contrast, the subsequent addition of molecular oxygen is spin-restricted, because the reactants initially reside on different spin manifolds (doublet radical cation and triplet ground-state O_2). The O_2 addition, therefore, requires a transition between spin surfaces *via* intersystem crossing (ISC) or surface hopping at a crossing point, rather than being strictly spin-forbidden by multiplicity rules. The rate and feasibility of such reactions are governed by the spin–orbit coupling matrix elements and the energetics of the minimum energy crossing point (MECP) between spin surfaces.[34,35]

To gain comprehensive understanding of the underlying ion–molecule reactions of amines under SIFT conditions and the behavior of the formed product ions, this work investigates the reactions of the primary amines *n*-propylamine and *n*-butylamine and the secondary amines dipropylamine and dibutylamine with the three positive reagent ions H_3O^+, NO^+ and $O_2^{+\bullet}$, reporting observed product ion ratios and reaction rate coefficients under SIFT conditions.

Experimental

Instrumentation

All experiments in this work were conducted on the Syft Tracer instrument (Syft Technologies Limited, Christchurch, New Zealand). The three positive reagent ions H_3O^+, NO^+, and $O_2^{+\bullet}$ were generated in a microwave discharge ion source and individually injected into the flow tube *via* a quadrupole mass filter in a fast sequence. The negative reagent ions did not produce any meaningful product ions and were therefore not investigated further. Nitrogen (purity 5.0, Messer Technogas, Prague, Czechia) was used as the carrier gas. The sample inlet cone and capillary were maintained at a constant temperature of 393 K to prevent analyte vapor condensation. The sample gas was introduced into the flow tube (393 K, 457 mTorr) at a constant sample gas flow of 18.5 sccm.

Chemicals and sample introduction

For the determination of product branching ratios and reaction rate coefficients, gaseous mixtures of *n*-propylamine, *n*-butylamine, dipropylamine and dibutylamine were prepared in Nalophan bags filled with either dry, clean air (from a zero-air generator UHP-10ZA-S, Parker, Gateshead, United Kingdom) or nitrogen. Several millilitres of analyte headspace were injected using plastic gas-tight syringes (Omnifix®, B. Braun, Bad Arolsen, Germany). All samples were at room temperature during the experiments.

For experiments investigating the effect of oxygen concentration on ion formation, individual diffusion tubes containing one of the four amines were prepared and placed individually in a laboratory bottle. The bottle was flushed with a constant

total flow of zero-air and nitrogen in varying proportions to adjust the oxygen concentration.

Dibutylamine (purity 99%), dipropylamine (purity 99%), *n*-butylamine (purity 99%), and *n*-propylamine (purity 98%) were purchased from Sigma-Aldrich. All chemicals were used without further purification.

Determination of reaction rate coefficients and observed product ion ratios

To determine the product ion ratios, full scan (FS) mass spectra were acquired over *m*/*z* 10–300 from gaseous samples of the four amines, alongside blanks from Nalophan bags containing zero-air or nitrogen only, for all three positive reagent ions. During FS acquisition, the Nalophan bag, initially spiked with the analyte vapor headspace, was then continuously flushed with zero-air or nitrogen, respectively, causing the analyte vapor concentrations to decrease over time. FS mass spectra were collected with a measurement time limit of 200 ms and an ion count limit of 10 000. The *m*/*z* range was chosen to capture secondary products such as dimers and adducts. The main product ions were assigned from the FS mass spectra.

For each reagent ion, the product ion ratios were calculated as individual product ion count rates divided by the sum of all product ion count rates and extrapolating plots of observed product ion ratios *versus* the count rates of the known major product ions to the limit of zero concentration (standard extrapolation procedure).

The reaction rate coefficients were determined relative to the proton transfer from H_3O^+, which is assumed to proceed at the collisional rate, k_c,[36] given the high exothermicity of the reactions above at least 226 kJ mol^{-1}.[37,38] For the remaining reagent ions, the relative rates were derived from the slopes of $[P^+]/[R^+]$ *versus* analyte vapor concentration in the limit of zero concentration,[39,40] where $[P^+]$ is the total product ion count rate and $[R^+]$ is the total reagent ion count rate (including all hydrates). The slopes were normalised to H_3O^+ to obtain relative rate coefficients, which were then converted to absolute values by multiplying the relative rate coefficients by k_c for H_3O^+, calculated from the parametrisation from Su and Chesnavich.[41]

Determination of equilibrium constants for the association reaction

For amine radical cations, adduct formation with O_2 after initial hydrogen shifts is a possible reaction mechanism (see reaction (11)), as also observed in this work (see below). As such adducts can potentially dissociate again, it is useful to determine the equilibrium constants for such reactions to provide insights into the reaction thermodynamics.

The equilibrium constant $K_{eq,n}$ for this reaction can be determined from the $(M + O_2)^{+\bullet}/M^{+\bullet}$ intensity ratio *versus* the local O_2 molecule density. Under the SIFT operating conditions (p^{SIFT} = 457 mTorr, T^{SIFT} = 393 K), the O_2 molecule density is calculated from the dilution of the sample gas ($\dot{V}_{sample}$ = 18.5 sccm) into the carrier gas ($\dot{V}_{carrier}$ = 128 sccm), multiplied by the total particle density inside the flow tube according to eqn (12), where ϕ_{O_2} is the oxygen volume fraction in the sample gas ϕ_{O_2} (0–21%). A linear fit of $(M + O_2)^{+\bullet}/M^{+\bullet}$ *versus* $[O_2]$ yields the equilibrium constant $K_{eq,n}$ (in m^3 per particle) given by eqn (13). To convert this to a dimensionless equilibrium constant K_{eq}^{Ref} referenced to standard pressure according to IUPAC recommendations (p^{Ref} = 1 bar) at the temperature of the experiment (T^{Ref} = 393 K), $K_{eq,n}$ is multiplied by the total particle density at the reference state. The change in Gibbs free energy is then calculated from eqn (14) using the gas constant *R*.

$$[O_2] = \phi_{O_2} \frac{\dot{V}_{sample}}{\dot{V}_{sample} + \dot{V}_{carrier}} \cdot \frac{p^{SIFT}}{k_B T^{SIFT}} \quad (12)$$

$$K_{eq,n} = \frac{\left[(M + O_2)^{+\bullet}\right]}{[M^{+\bullet}][O_2]} \quad (13)$$

$$K_{eq}^{Ref} = K_{eq,n} N^{Ref} = K_{eq,n} \cdot \frac{p^{Ref}}{k_B T^{Ref}} = \exp\left(-\frac{\Delta G^{Ref}}{R T^{Ref}}\right) \quad (14)$$

DFT calculations

All quantum chemistry calculations based on DFT were carried out using the ORCA 6.1 program package.[42–44] To assess the reaction mechanism and gas-phase structure of observed $(M + O_2)^{+\bullet}$ adducts (see below), initial structures for the radical cations of *n*-propylamine, *n*-butylamine, dipropylamine, and dibutylamine as well as the oxygen molecule and all possible reaction products from intramolecular hydrogen rearrangement and subsequent O_2 addition, or alternatively, adducts between the radical cations and O_2 bound by van der Waals interactions, were drawn using the AVOGADRO software.[45] Geometries were then optimised using the B3LYP functional and the 6-311++G(d,p) basis set and a D4 correction.[46–48] All open-shell species, including the conventional amine radical cations, the distonic radical cation isomers, and the $(M + O_2)^{+\bullet}$ adducts, were treated as doublets. Quartet states were not explicitly explored, as the experimentally observed product ions correspond to singly charged radicals and the lowest-energy peroxyl-type adducts of organic radicals with O_2 are expected to have doublet multiplicity. Although B3LYP is not the most recent general-purpose functional, it has been widely and successfully applied in gas-phase ion chemistry to describe conventional and distonic radical cations as well as related peroxyl systems. For example, Flammang *et al.* used B3LYP/6-31+G(d,p) and B3LYP/6-311++G(3df,2p) to characterise the energetics of ionised benzonitrile and its distonic isomers in the gas phase, obtaining reliable relative stabilities and ionisation energies.[49] Tomazela *et al.* likewise employed B3LYP/6-311+G(d,p) in their definition and analysis of 'distonoid' radical cations.[50] Kirk *et al.* combined B3LYP with higher-level (U)CCSD(T) calculations to model charge-tagged phenylperoxyl radicals and their O_2 reactivity.[31] In the present work, our focus is on relative energies and qualitative trends between conventional and distonic amine radical cations and their $(M + O_2)^{+\bullet}$ adducts. For all open-shell species, $\langle S^2 \rangle$ values below 0.755

confirm negligible spin contamination and support the reliability of the chosen level of theory for describing these double states. Conformers were generated with CREST[51] and re-optimised. Gibbs energies were derived from harmonic frequencies within the rigid-rotor-harmonic-oscillator (RRHO)[52] approximation at 393 K. The same level of theory was used to compute normal-mode vibrational frequencies and thermodynamic quantities of all product ions. For each ion, plausible conformers were considered, and the lowest energy structures were selected. For all reactions, the enthalpy, entropy and Gibbs energy changes were evaluated at 393.15 K and standard pressure (1 bar). Polarizabilities and dipole moments were determined for the neutral amine molecules at the same level of theory.

Results and discussion

The data that support the findings of this study are openly available in the National Data Repository at https://data.narodni-repozitar.cz/heyrovsky/datasets/zkt15-an280.[53]

Compound properties

Table 1 lists the proton affinity (PA) and ionisation energy (IE) of the four amines, as well as their polarisabilities (α), dipole moments (D), and calculated k_c for H_3O^+, NO^+ and $O_2^{+\bullet}$ at 393 K.

Since all proton affinities substantially exceed that of water (691 kJ mol^{-1}),[38] proton transfer from H_3O^+ is strongly exothermic for each amine. Likewise, all ionisation energies are below those of NO (9.26 eV) and O_2 (12.07 eV),[38] making charge transfer exothermic for all compounds.

Reaction rate coefficients and observed product ion ratios

The observed relative reaction rate coefficients and observed product ion ratios for the reactions of *n*-propylamine, *n*-butylamine, dipropylamine and dibutylamine with H_3O^+, NO^+ and $O_2^{+\bullet}$ are shown in Table 2 and Fig. 1. All reaction rate coefficients have been determined in both dry and humid air.

H_3O^+ reactions. Under dry conditions, the reactions of H_3O^+ are fastest among the three positive reagent ions. This aligns with the established observation that sufficiently exothermic proton transfer reactions (typically >25 kJ mol^{-1}) proceed at the collisional rate.[36] In humid air, however, the observed reaction rate coefficients decrease by about 5–30% due to the hydration of H_3O^+. Under such conditions, $H_3O^+(H_2O)$ is the predominant reagent ion, accompanied by both H_3O^+ and $H_3O^+(H_2O)_2$, resulting in slower reactions compared to dry conditions.

Table 2 Observed reaction rate coefficients for the reactions of the investigated amines with H_3O^+, NO^+ and $O_2^{+\bullet}$ in dry or humid air

	k (H_3O^+) in 10^{-9} cm^3 s^{-1}		k (NO^+) in 10^{-9} cm^3 s^{-1}		k ($O_2^{+\bullet}$) in 10^{-9} cm^3 s^{-1}	
Compound	Dry	Humid	Dry	Humid	Dry	Humid
n-Propylamine	2.21	1.97	1.88	1.88	1.61	2.06
n-Butylamine	2.42	1.96	2.20	2.42	2.03	2.42
Dipropylamine	2.44	2.17	2.17	2.44	2.27	2.44
Dibutylamine	2.59	1.84	2.59	2.59	2.28	2.54

For all four amines, the dominant product ion is the protonated molecule. In addition, all amines yield NH_4^+ at m/z 18, likely from fragmentation of the protonated molecule, consistent with the large difference in proton affinities between water and the neutral amines. Similar fragments have been reported before for *n*-propylamine, 2-propylamine and *n*-butylamine in SIFT-MS.[55]

Notably, both secondary amines form the $(M - H)^+$ ion, that is an uncommon product ion for the proton transfer channel. Nevertheless, such product ions have also been reported for dimethylamine and trimethylamine in PTR-MS studies.[56] In agreement with the present study, methylamine as a primary amine does not form such ions in PTR-MS.

No substantial differences are observed between the reactions in air and in nitrogen.

NO^+ reactions. The reactions of NO^+ with all four amines proceed at or close to the collision rate. In contrast to the H_3O^+ reactions, no significant effect of humidity on the observed reaction rate coefficients is evident, since NO^+ remains the dominant reagent ion even under humid conditions. The reaction rate coefficient for the reactions with *n*-butylamine even exceed the theoretical collisional limit, which has been reported before in selected ion flow-drift tube SIFDT-MS for charge transfer from NO^+ and $O_2^{+\bullet}$ to isoprene at elevated interaction energies.[57]

In nitrogen, *n*-propylamine and *n*-butylamine product ions are dominated by the radical cation $M^{+\bullet}$ (45–50%) and $(M - H)^+$ from hydride ion transfer (50–55%), both of which have been reported in SIFT-MS before for primary amines.[55] Both secondary amines also produce a single prominent fragment alongside $M^{+\bullet}$ and $(M - H)^+$: $C_4H_{10}N^{+\bullet}$ (m/z 72) for dipropylamine, corresponding to ethyl loss, and $C_5H_{12}N^{+\bullet}$ (m/z 86) for dibutylamine, corresponding to propyl loss. No stable adducts between NO^+ and the neutral amines are observed, consistent

Table 1 Proton affinities (PA),[37] ionisation energies (IE),[54] polarisabilities (α), dipole moments (D) and ion–molecule collisional rate coefficients (k_c) calculated from the parametrisation of Su and Chesnavich[41] for a temperature of 393 K

Compound	PA (kJ mol^{-1})	IE (eV)	α (10^{-24} cm^3)	D (Debye)	k_c (H_3O^+) (10^{-9} cm^3 s^{-1})	k_c (NO^+) (10^{-9} cm^3 s^{-1})	k_c ($O_2^{+\bullet}$) (10^{-9} cm^3 s^{-1})
n-Propylamine (59)	917.8	8.78	7.21	1.27	2.21	1.88	1.84
n-Butylamine (73)	921.5	8.71	9.07	1.42	2.42	2.04	1.99
Dipropylamine (101)	962.3	7.84	12.63	1.08	2.44	2.03	1.98
Dibutylamine (129)	968.5	7.69	16.51	0.90	2.59	2.14	2.08

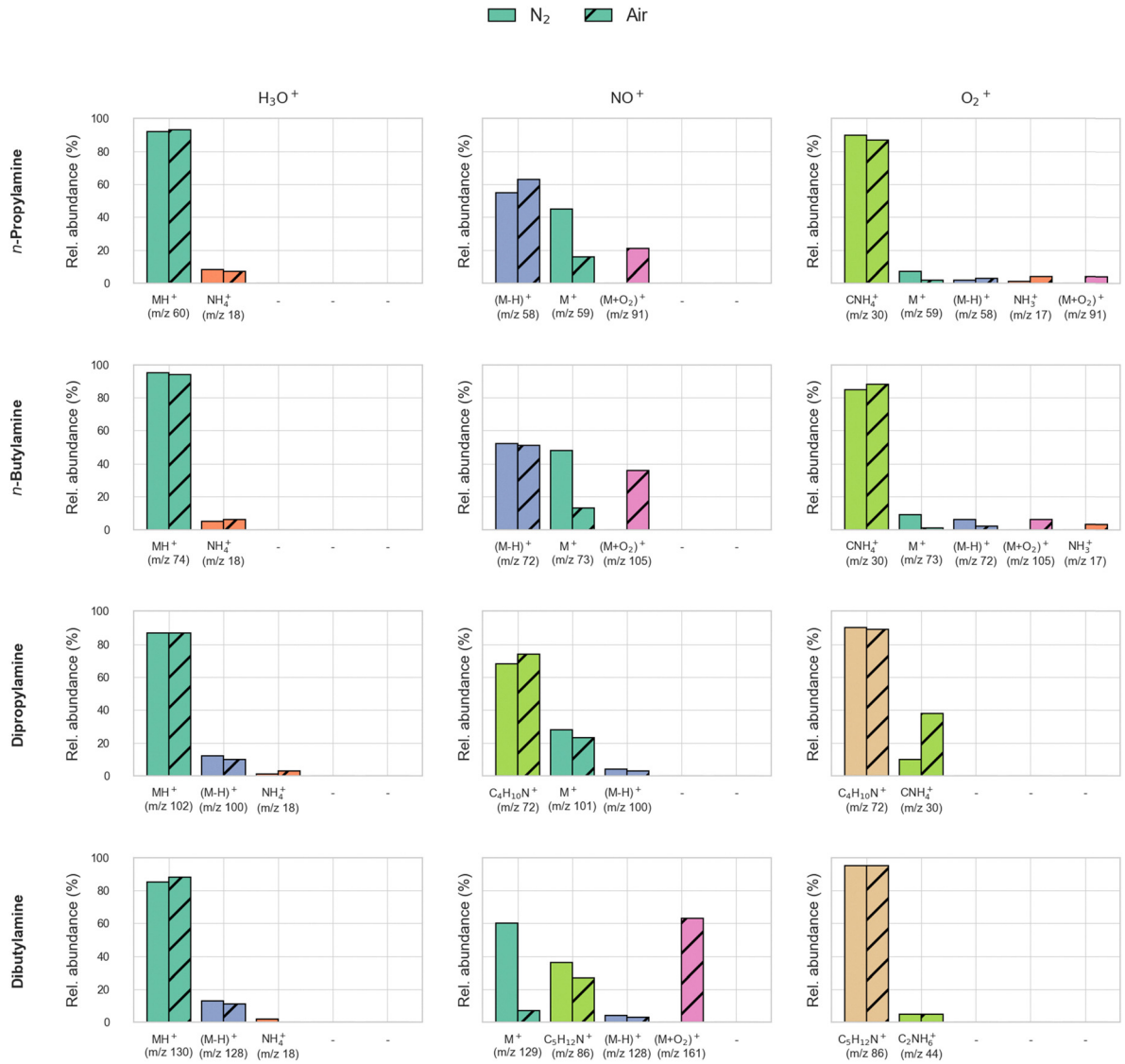

Fig. 1 Observed product ion ratios of the reactions of the investigated amines with H_3O^+, NO^+ and $O_2^{+\bullet}$ using either air or nitrogen as sample make up gas.

with the large differences in ionisation energies between the amines and NO.

When air is used as sample make up gas instead of nitrogen, notable shifts in observed product ion ratios occur. For the primary amines, observed $M^{+\bullet}$ ion ratios decrease as that of $(M - H)^+$ remains constant and substantial formation of an additional product ion $(M + O_2)^{+\bullet}$ can be observed. In the secondary amines, dipropylamine exhibits only a slight increase in the observed fragment $C_4H_{10}N^{+\bullet}$ ion ratio, with a corresponding decrease in $M^{+\bullet}$ and little $(M + O_2)^{+\bullet}$ formation. In contrast, dibutylamine forms $(M + O_2)^{+\bullet}$ in substantial amounts alongside its dominant fragment $C_5H_{12}N^{+\bullet}$. In all cases, the observed $(M + O_2)^{+\bullet}$ ion ratio is $<1\%$ in nitrogen, suggesting that the reaction mechanism depends on the presence of molecular oxygen. While adducts with polar molecules such as water, or adducts of the neutrals with NO^+, are often observed in SIFT experiments,[23] O_2 adducts are typically short-lived and therefore not observed. Their detection in the present work is therefore notable and discussed in more detail below.

Note that the neutral products of reactions between reagent ions NO^+ and the amines are present in the flow tube at a negligible concentration ($<10^4$ cm^{-3}).[58] Even if NO thus formed were oxidised to NO_2, it would still react only with one ion (or fewer) in a million. Therefore, no NO_2-related ions were observed in the mass spectra, as secondary reactions involving neutral products can be disregarded.

$O_2^{+\bullet}$ reactions. The reactions of $O_2^{+\bullet}$ with all four amines proceed at or close to the collisional rate, with modest increases under humid conditions. Except for the reaction with *n*-propylamine in dry air, all reaction rate coefficients again exceed the theoretical collisional rate.

In contrast to NO^+ and H_3O^+, the strong exothermicity (3.3–4.3 eV) of charge transfer from $O_2^{+\bullet}$ causes extensive

fragmentation, and only minor amounts of $M^{+\bullet}$ or $(M - H)^+$ are observed even in nitrogen. In nitrogen, for the primary amines *n*-propylamine and *n*-butylamine, the most abundant fragment occurs at *m/z* 30, isobaric with residual NO^+ reagent ions but clearly correlated with amine vapour concentration, which is thus assigned as a product ion. As also a small contribution

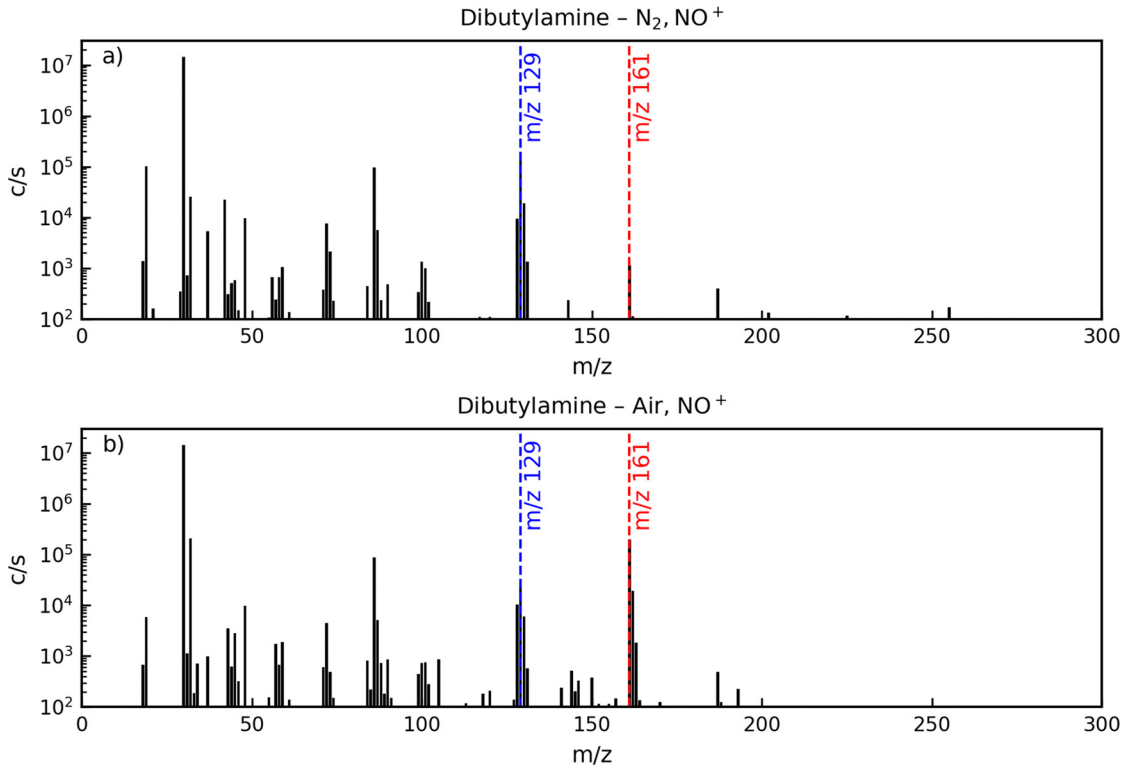

Fig. 2 Comparison of SIFT mass spectra of dibutylamine using NO^+ as reagent ion in (a) nitrogen and (b) zero-air.

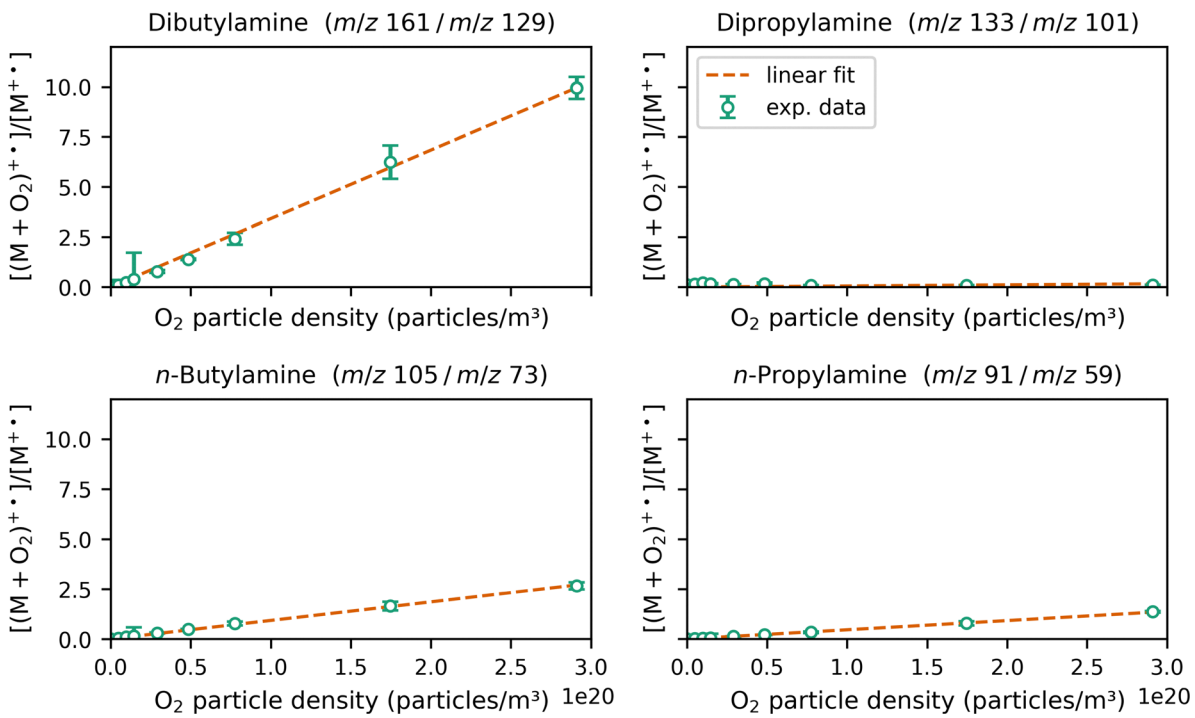

Fig. 3 Ratio of $(M + O_2)^{+\bullet}$ to $M^{+\bullet}$ depending on oxygen molecule density in the flow tube for all four amines at T = 393 K. The red dashed line represents a linear fit to the mean values of the ratio of signal intensities. The error bars depict the standard deviation of five measurements.

from *m*/*z* 31, that is also concentration-dependent, can be found, the observed product ions are assigned as $CNH_4^{+\bullet}$ and its ^{13}C-isotologue, which is a typical fragment of distonic amine radical cations[27,59] and has been observed as fragment of *n*-propylamine and *n*-butylamine in reactions with $O_2^{+\bullet}$ before.[55] These are accompanied by $NH_3^{+\bullet}$ and smaller contributions form alkyl-containing fragments, with $(M + O_2)^{+\bullet}$ essentially absent. For the secondary amines, dipropylamine fragmentation yields mainly $C_4H_{10}N^{+\bullet}$ (*m*/*z* 72), with $CNH_4^{+\bullet}$ (*m*/*z* 30) as minor product ion, while dibutylamine fragmentation yields almost exclusively $C_5H_{12}N^{+\bullet}$ (*m*/*z* 86) alongside a minor $C_2NH_6^{+\bullet}$ (*m*/*z* 44) fragment. The latter, like $CNH_4^{+\bullet}$, is a common fragment of distonic amine radical cations.[27,59]

When air is used as the sample make up gas, only minor $(M + O_2)^{+\bullet}$ signals can be detected. This aligns with the observations from the NO^+ reactions, where the sum of $M^{+\bullet}$ and $(M + O_2)^{+\bullet}$ remains almost constant upon switching from nitrogen to air. Since the amount of $M^{+\bullet}$ is already very small in nitrogen when using $O_2^{+\bullet}$ as reagent ion, only minor contributions from $(M + O_2)^{+\bullet}$ result when switching to zero-air.

Oxygen adduct formation

The formation of the oxygen adduct $(M + O_2)^{+\bullet}$, particularly in the NO^+ reactions, is notable as it represents an unusual product ion under SIFT conditions. Substantial ion yields are observed only when zero-air is used as the sample make up gas, as shown by the two exemplary mass spectra of dibutylamine in Fig. 2. In nitrogen, the mass spectra contain only $M^{+\bullet}$, $(M - H)^+$, and the characteristic fragments such as $C_5H_{12}N^{+\bullet}$ (*m*/*z* 86). This behaviour indicates that the formation of $(M + O_2)^{+\bullet}$ depends on the availability of molecular oxygen.

To investigate this further, the mixing ratio between air and nitrogen was varied and the intensities of $(M + O_2)^{+\bullet}$ and $M^{+\bullet}$ were monitored in selected ion monitoring (SIM) mode. The oxygen concentration is calculated in this experiment from the mixing ratio of air (containing 21% O_2) and nitrogen (containing 0% O_2). Fig. 3 shows that for increasing oxygen concentrations, the ratio of $(M + O_2)^{+\bullet}$ to $M^{+\bullet}$ in the NO^+ reactions strongly increases, with dipropylamine showing only small amounts of $(M + O_2)^{+\bullet}$ even in air. The other three amines also differ markedly in the observed product ion ratio of $(M + O_2)^{+\bullet}$: in pure zero-air (*i.e.*, 21% O_2), dibutylamine yields about ten times more $(M + O_2)^{+\bullet}$ than $M^{+\bullet}$, *n*-butylamine about 2.7 times more, and *n*-propylamine only about 1.3 times more. In comparison, the $(M + O_2)^{+\bullet}$ signal for dipropylamine is only about 10% of the corresponding $M^{+\bullet}$ signal.

The total amount of $M^{+\bullet}$ + $(M + O_2)^{+\bullet}$ remains approximately constant, indicating that $(M + O_2)^{+\bullet}$ is formed from $M^{+\bullet}$ in the presence of molecular oxygen. The linear increase of the $(M + O_2)^{+\bullet}$/$M^{+\bullet}$ ratio in Fig. 3 with increasing oxygen concentration aligns with an equilibrium reaction rather than a simple first-order reaction, which would yield an exponential decay of $M^{+\bullet}$ with increasing oxygen concentration. This assumption is supported by the semi-log plots of $M^{+\bullet}$ and $(M + O_2)^{+\bullet}$ intensities *versus* oxygen concentrations in Fig. 4, where the experimental data deviate from linearity (*i.e.*, exponential decay) at high oxygen concentrations.

Using the procedure described in the Methods section, the equilibrium coefficient K_{eq}^{Ref} and Gibbs energy ΔG^{Ref} values for

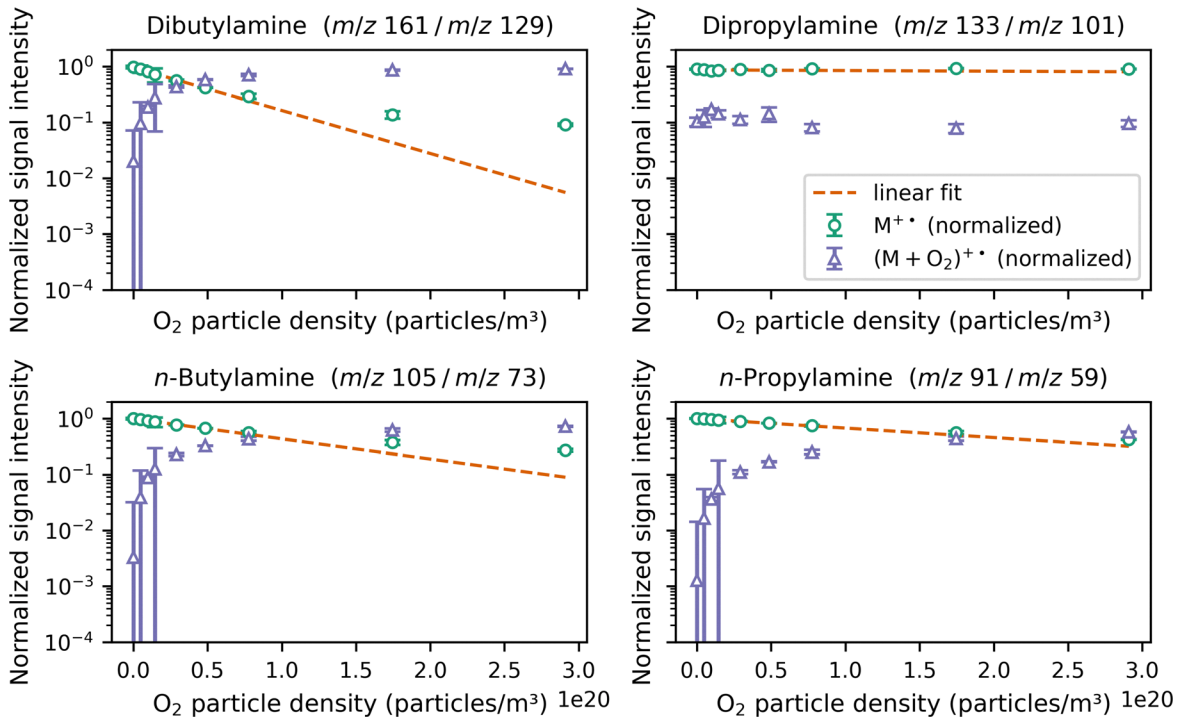

Fig. 4 Dependence of $(M + O_2)^{+\bullet}$ (green) and $M^{+\bullet}$ (blue) signal intensity on oxygen molecule density in the flow tube for all four amines at T = 393 K. The red dashed line represents an exponential fit to the mean values of $M^{+\bullet}$ (*i.e.* the reagent) signal intensities. The error bars depict the standard deviation of five measurements.

Table 3 Observed equilibrium constants under quasi-steady-state conditions obtained from the slope of the experimentally determined $(M + O_2)^{+\bullet}/M^{+\bullet}$ ratio depending on oxygen concentration and calculated Gibbs energy changes at T = 393.15 K and standard pressure of 1 bar

Compound	Obtained equilibrium constant K_{eq}^{Ref} at 393 K and 1 bar	Gibbs energy change ΔG^{Ref} at 393 K and 1 bar in kJ mol^{-1}
n-Propylamine	86 000	−37.13
n-Butylamine	170 000	−39.42
Dipropylamine	10 000	−30.25
Dibutylamine	640 000	−43.68

all four amine reactions can be obtained for the reference state of 1 bar and 393 K (see Table 3). The obtained Gibbs energy changes are negative for all four amines (−30.25 kJ mol^{-1} to −43.68 kJ mol^{-1}), substantially exceeding the mean translational kinetic energy at 393 K (about 5 kJ mol^{-1}). However, these observed experimental ΔG^{Ref} values do not align with those from quantum chemical calculations (see Methods section) for van der Waals-bound adducts between the radical cation and O_2 (Fig. 5). The computed Gibbs energies show that such adduct formation is exothermic for all four amines, but the reaction entropies are strongly negative, favouring the separate radical cation and molecular oxygen. This pronounced negative entropy contribution arises because the reaction reduces the number of independent gas-phase particles: two reactants combine to yield a single product. Such a decrease in entropy is typical for association reactions in the gas phase, and it can significantly affect the equilibrium even when the reaction is energetically favourable.

Thus, the overall Gibbs energy changes for the formation of a van der Waals-bound adduct are strongly positive, suggesting that such ions are an unlikely explanation of the occurring $(M + O_2)^{+\bullet}$ signals. We emphasize that the secondary reaction with O_2 should be regarded as a quasi-steady state rather than true thermodynamic equilibrium during the flow tube residence time. As described above, the O_2 addition involves ISC, which is often slow in light-atom organic systems.[34,35] Therefore, the spin restriction can further slow the secondary O_2 addition reaction, reinforcing a quasi-steady-state behavior rather than full equilibration. Although we did not explicitly compute spin–orbit coupling (SOC) matrix elements for the present systems, previous theoretical studies on radical reactions report SOC values sufficient to enable intersystem crossing under thermal, collisional conditions.[34,35] In view of the millisecond residence time and the collision frequency in the SIFT flow tube, surface crossing and subsequent O_2 addition should therefore be kinetically feasible within the present experiment. As a result, the observed product ion ratios may underestimate the true equilibrium constant, and the

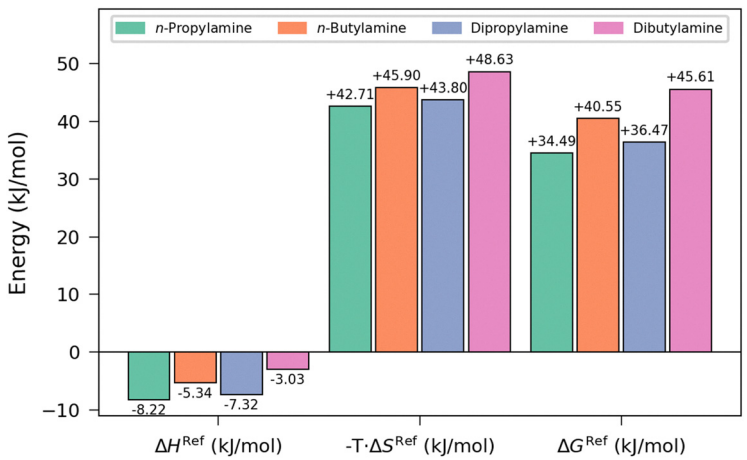

Fig. 5 Reaction enthalpies ΔH^{Ref}, reaction entropy terms $T{\cdot}\Delta S^{Ref}$ and Gibbs energy changes ΔG^{Ref} for the formation of an adduct between the radical cation and molecular oxygen bound by van der Waals interactions at T = 393.15 K.

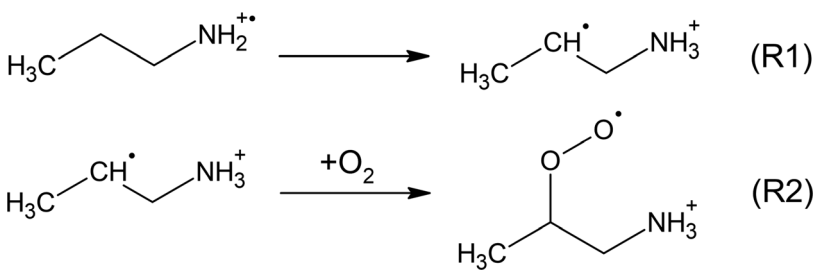

Fig. 6 Reaction scheme of intramolecular 1,3-hydrogen shift (R1) followed by addition of O_2 (R2) to the distonic *n*-propylamine radical cation as an example.

ΔG^{Ref} values derived from these ratios may appear slightly too endergonic compared to the true thermodynamic values. Therefore, these represent effective, apparent thermodynamic parameters under kinetic constraints.

While the thermodynamic analysis rules out a simple adduct from van der Waals interactions as the dominant contributor to the $(M + O_2)^{+\bullet}$ signal, it does not explain the different observed product ion ratios of $M^{+\bullet}$ and $(M + O_2)^{+\bullet}$ for the four amines. To address this, we next consider a mechanistic pathway supported by literature results: an intramolecular hydrogen shift in the radical cation followed by O_2 addition at the carbon-centered radical site. Amine radical cations can undergo a hydrogen shift from a carbon atom to the nitrogen atom – where the positive charge remains – according to R1 in Fig. 6.[24,25] The resulting distonic radical cation can then react with molecular oxygen at the carbon-centred radical site according to R2 in Fig. 6.[28,29]

For the primary amines studied here, optimised geometries with negative ΔG^{Ref} for the hydrogen shift step were found

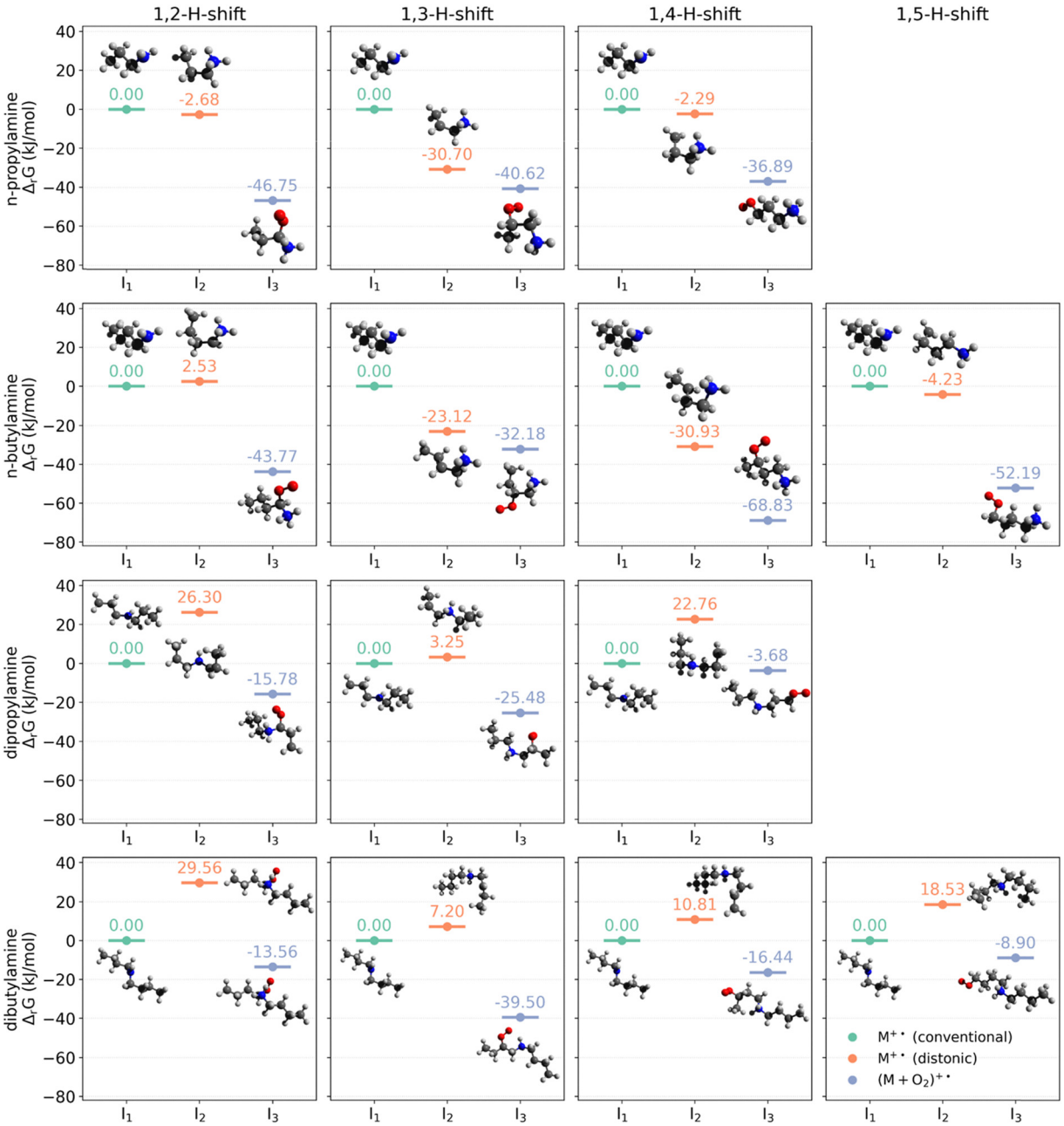

Fig. 7 Relative Gibbs energy levels of independently optimised species for all four amines at 393 K and 1 bar. For each amine, three stationary points are shown as horizontal energy levels: the conventional radical cation (I_1, set to 0), the corresponding distonic radical cation (I_2), and $(M + O_2)^{+\bullet}$ after addition of molecular oxygen to the distonic radical cation (I_3). The optimised structures are displayed alongside their corresponding energy levels only for visualisation. I_1 and I_2 were optimised without O_2, whereas I_3 included one bound O_2 molecule. The diagram illustrates the relative thermodynamic ordering of these stationary points only: no transition states, pre-reactive complexes, or continuous reaction pathways are implied.

(see Fig. 7), indicating a thermodynamically favourable rearrangement. In contrast, no such exergonic rearrangements were found for the secondary amines: for dipropylamine and dibutylamine, the lowest energy structure corresponds to a 1,3-H shift, lying at least 3 and 7 kJ mol^{-1}, respectively, above the initially formed radical cation. Nevertheless, for all four amines, the addition of molecular oxygen to the distonic radical cation (R2) is exergonic, rendering the combined reaction (R1 followed by R2) exergonic. Attempts to find stable N-bound oxygen adducts without an H-shift were unsuccessful, supporting a mechanism in which $(M + O_2)^{+\bullet}$ arises from hydrogen rearrangement followed by O_2 addition. For the secondary amines, the computed differences in the Gibbs energy between the conventional radical cation and the lowest energy $(M + O_2)^{+\bullet}$ structure are −25.48 kJ mol^{-1} (dipropylamine) and −39.50 kJ mol^{-1} (dibutylamine), both for the 1,3-H shift. These values reasonable agree with the Gibbs energy changes from the observed experimental equilibrium constants under quasi-steady-state conditions. For the primary amines, the lowest-energy structures (−46.75 kJ mol^{-1} for *n*-propylamine; −68.83 kJ mol^{-1} for *n*-butylamine), exceed those observed experimental ΔG^{Ref} values. In these cases, the lowest energy adduct may not establish the equilibrium with the conventional radical cation but with the distonic ion due to its lower Gibbs energy. The ΔG^{Ref} differences for these equilibria (−37.90 kJ mol^{-1} for *n*-butylamine, 1,4-H shift; −44.07 kJ mol^{-1} for *n*-propylamine, 1,2-H shift) align better with the experiment. Dipropylamine shows the smallest computed ΔG^{Ref}, indicating that O_2 adduct formation is least favoured, consistent with its low $(M + O_2)^{+\bullet}$ yield.

Note that Shiels *et al.* have shown that addition reactions of distonic radical ions can proceed *via* weakly bound pre-reactive complexes (PRCs), with the kinetics governed by the forward PRC to transition state (TS) barrier. This barrier depends on a multidimensional interplay of electrostatic and geometric factors, including charge-radical separation, the orientation of the TS dipole relative to the internal electric field, and, in related systems, properties such as the electron affinity of the radical cation or the ionisation energy of the neutral molecule.[33,60] In the present system, the ionisation energy of the neutral (O_2) remains constant, and only the magnitudes of the dipole moments of the neutral precursors are available, which do not show a consistent trend in the $(M + O_2)^{+\bullet}$ formation efficiencies. The particularly low O_2 reactivity of dipropylamine may therefore result from a comparatively high forward barrier for the PRC to adduct conversion.

However, kinetic effects might also contribute to the less efficient formation of $(M + O_2)^{+\bullet}$ in dipropylamine. The intramolecular H-shift barrier is higher for secondary than for primary amines.[24] Furthermore, the hydrogen shift usually proceeds *via* cyclic transition states (*e.g.* six-membered rings in 1,5-H shifts and five-membered rings in 1,4-H shifts), with 1,5-H shifts typically having lower activation barriers due to reduced ring strain.[24,61] Dipropylamine can undergo only a 1,4-H shift, whereas dibutylamine can also undergo a 1,5-H shift, potentially explaining that dipropylamine has lower rearrangement efficiency within the experimental timescale. Such kinetic hindrance could also account for residual discrepancies between computed and observed experimental ΔG^{Ref} values (see Table 3), if the equilibrium is not fully established. Furthermore, a more complex reaction mechanism involving additional intermediates such as adducts with NO^+ or another intermediate oxygen adducts cannot be excluded. Nevertheless, the collective data supports a reaction mechanism in which $(M + O_2)^{+\bullet}$ forms *via* hydrogen shift followed by O_2 addition rather than *via* a simple van der Waals-bound adduct.

Additional insights on this reaction mechanism could be obtained from exposing the amine radical cations to varying, but – in the timescale of the experiment – homogeneous electric fields. This could probe whether ion heating substantially affects the formation of $M^{+\bullet}$ and $(M + O_2)^{+\bullet}$. Also, experimental determination of their ion mobilities, benchmarked against ion mobility calculations (*e.g.* from MobCal-MPI[62] or IMoS[63]) on both the conventional and possible distonic radical cations and their O_2 adducts, could provide more insight into the actual gas-phase structures of radical cations formed by the studied amines. For both experiments, selected ion flow-drift tube SIFDT-MS[64,65] studies would be suitable due to the similar setup to the SIFT-MS ensuring similar operating conditions and ionisation settings. Such studies, however, are out of the scope of this work.

Conclusion

In this study, the product ion formation of selected primary and secondary amines in SIFT-MS was investigated using the three positive reagent ions H_3O^+, NO^+ and $O_2^{+\bullet}$. Across all three reagent ions, the reaction rate coefficients are at or close to the collisional limit, consistent with the high exothermicity of these reactions. With H_3O^+, proton transfer predominantly yields the protonated molecule. Charge transfer with $O_2^{+\bullet}$ produces mainly fragment ions of the radical cation. In contrast, NO^+ reactions in zero-air as sample make up gas generate unusual product ions (nominal mass + 32) for all amines with different observed product ion ratios, suggesting adduct formation between the radical cation and molecular oxygen. While the experimental data suggest an equilibrium reaction, quantum chemistry modelling indicates that van der Waals-bound adducts are not thermodynamically stable at the instrument temperature (393 K). Instead, a possible reaction mechanism involves intramolecular hydrogen shift within the radical cation followed by O_2 addition. The trend in computed Gibbs energy changes for these reactions aligns well with those obtained from the observed experimental equilibrium constants under quasi-steady-state conditions, explaining the different observed product ion ratios for $(M + O_2)^{+\bullet}$ formation. The remaining differences may reflect higher activation barriers for certain intramolecular hydrogen shifts, although a more complex reaction mechanism involving other adducts cannot be excluded.

Future follow-up experiments in SIFDT-MS could provide more detailed mechanistic insights about the reaction mechanism of $(M + O_2)^{+\bullet}$ formation. The homogeneous axial electric

field across the entire flow tube enables control of ion kinetic energy and, *via* collisional heating, internal energy. Systematically varying the electric field strength could reveal whether ion heating leads to either dissociation of $(M + O_2)^{+\bullet}$, or even more efficient reactions due to excitation, allowing them to overcome an activation barrier. Complementary ion mobility calculations on feasible structures for the radical cation may provide more insights into their structures and thus into possible arrangement reactions. While such studies are beyond the scope of the present work, they would substantially advance understanding the reaction mechanism that governs product ion formation of the investigated amines.

Author contributions

Christoph Schaefer: methodology, validation, formal analysis, investigation, data curation, visualisation, writing – original draft; Kseniya Dryahina: methodology, investigation, validation, writing – review & editing; Patrik Španěl: conceptualisation, methodology, software, resources, funding acquisition, supervision, writing – review & editing; Mark J. Perkins: conceptualisation, writing – review & editing; Vaughan S. Langford: conceptualisation, writing – review & editing.

Conflicts of interest

There are no conflicts to declare.

Data availability

All relevant data supporting this study can be found in the National Data Repository at https://data.narodnirepozitar.cz/heyrovsky/datasets/zkt15-an280, including data on observed product ion branching, reaction rate coefficients and ORCA output files for all optimized ion and neutral species.

Acknowledgements

The authors acknowledge the assistance provided by the Advanced Multiscale Materials for Key Enabling Technologies project, supported by the Ministry of Education, Youth, and Sports of the Czech Republic. Project No. CZ.02.01.01/00/22_008/0004558, Co-funded by the European Union. Patrik Španěl acknowledges the Praemium Academiae award by the Czech Academy of Sciences.

References

1 European Medicines Agency, *Assessment report: Nitrosamine impurities in human medicinal products*, Report EMA/369136/2020, European Medicines Agency, Amsterdam, The Netherlands, 2020.
2 H. Akkaraju, R. Tatia, S. S. Mane, A. B. Khade and S. J. Dengale, A comprehensive review of sources of nitrosamine contamination of pharmaceutical substances and products, *Regul. Toxicol. Pharmacol.*, 2023, **139**, 105355.
3 J. Schlingemann, M. J. Burns, D. J. Ponting, C. Martins Avila, N. E. Romero, M. A. Jaywant, G. F. Smith, I. W. Ashworth, S. Simon, C. Saal and A. Wilk, The Landscape of Potential Small and Drug Substance Related Nitrosamines in Pharmaceuticals, *J. Pharm. Sci.*, 2023, **112**, 1287–1304.
4 U.S. Food and Drug Administration, *Control of Nitrosamine Impurities in Human Drugs: Guidance for Industry*, Report FDA-2020-D-1530, Center for Drug Evaluation and Research, U.S. Food and Drug Administration, Silver Spring, MD, 2024.
5 International Agency for Research on Cancer, *IARC Monographs on the Evaluation of the Carcinogenic Risk of Chemicals to Humans. Volume 17: Some N-Nitroso Compounds*, International Agency for Research on Cancer, Lyon, France, 1978.
6 International Council for Harmonisation of Technical Requirements for Pharmaceuticals for Human Use, *ICH harmonised guideline: Assessment and control of DNA reactive (mutagenic) impurities in pharmaceuticals to limit potential carcinogenic risk*, Report EMA/CHMP/ICH/83812/2013, ICH, Geneva, Switzerland, 2023.
7 S. R. Shewchuk, A. Mukherjee and A. K. Dalai, Selective carbon-based adsorbents for carbon dioxide capture from mixed gas streams and catalytic hydrogenation of CO_2 into renewable energy source: A review, *Chem. Eng. Sci.*, 2021, **243**, 116735.
8 I. Eide-Haugmo, O. G. Brakstad, K. A. Hoff, K. R. Sørheim, E. F. da Silva and H. F. Svendsen, presented in part at the Greenhouse Gas Control Technologies 9: Proceedings of the 9th International Conference on Greenhouse Gas Control Technologies (GHGT-9), Washington, DC, USA, 2009.
9 R. S. Andre, L. A. Mercante, M. H. M. Facure, R. C. Sanfelice, L. Fugikawa-Santos, T. M. Swager and D. S. Correa, Recent Progress in Amine Gas Sensors for Food Quality Monitoring: Novel Architectures for Sensing Materials and Systems, *ACS Sens.*, 2022, **7**, 2104–2131.
10 B. S. Sivamaruthi, P. Kesika and C. Chaiyasut, A narrative review on biogenic amines in fermented fish and meat products, *J. Food Sci. Technol.*, 2021, **58**, 1623–1639.
11 A. Dehaut, S. Duthen, T. Grard, F. Krzewinski, A. N'Guessan, A. Brisabois and G. Duflos, Development of an SPME-GC-MS method for the specific quantification of dimethylamine and trimethylamine: use of a new ratio for the freshness monitoring of cod fillets, *J. Sci. Food Agric.*, 2016, **96**, 3787–3794.
12 Z. Karpas, B. Tilman, R. Gdalevsky and A. Lorber, Determination of volatile biogenic amines in muscle food products by ion mobility spectrometry, *Anal. Chim. Acta*, 2002, **463**, 155–163.
13 N. S. Turna, R. A. Chung and L. McIntyre, A review of biogenic amines in fermented foods: Occurrence and health effects, *Heliyon*, 2024, **10**, e24501.
14 F. Gardini, Y. Özogul, G. Suzzi, G. Tabanelli and F. Özogul, Technological Factors Affecting Biogenic Amine Content in Foods: A Review, *Front. Microbiol.*, 2016, **7**, 1218.

15 M. T. Veciana-Nogues, M. S. Albala-Hurtado, M. Izquierdo-Pulido and M. C. Vidal-Carou, Validation of a gas-chromatographic method for volatile amine determination in fish samples, *Food Chem.*, 1996, **57**, 569–573.
16 J. Namiesnik, A. Jastrzebska and B. Zygmunt, Determination of volatile aliphatic amines in air by solid-phase microextraction coupled with gas chromatography with flame ionization detection, *J. Chromatogr. A*, 2003, **1016**, 1–9.
17 A. Fekete, A. K. Malik, A. Kumar and P. Schmitt-Kopplin, Amines in the Environment, *Crit. Rev. Anal. Chem.*, 2010, **40**, 102–121.
18 C. Viana, G. M. Zemolin, F. O. Lima, L. M. de Carvalho, C. B. G. Bottoli and R. P. Limberger, High-performance liquid chromatographic analysis of biogenic amines in pharmaceutical products containing Citrus aurantium, *Food Addit. Contam.,:Part A*, 2013, **30**, 634–642.
19 G. Vanhoenacker, E. Dumont, F. David, A. Baker and P. Sandra, Determination of arylamines and aminopyridines in pharmaceutical products using in-situ derivatization and liquid chromatography-mass spectrometry, *J. Chromatogr. A*, 2009, **1216**, 3563–3570.
20 C. You, T. Ho, V. Rucker, J. Yeh and L. Wang, A simple and universal headspace GC-FID method for accurate quantitation of volatile amines in pharmaceuticals, *Anal. Methods*, 2023, **15**, 4427–4433.
21 V. S. Langford, K. Dryahina and P. Španěl, Robust Automated SIFT-MS Quantitation of Volatile Compounds in Air Using a Multicomponent Gas Standard, *J. Am. Soc. Mass Spectrom.*, 2023, **34**, 2630–2645.
22 D. Smith, P. Španěl, N. Demarais, V. S. Langford and M. J. McEwan, Recent developments and applications of selected ion flow tube mass spectrometry (SIFT-MS), *Mass Spectrom. Rev.*, 2022, **44**, 101–134.
23 D. Smith, M. J. McEwan and P. Španěl, Understanding Gas Phase Ion Chemistry Is the Key to Reliable Selected Ion Flow Tube-Mass Spectrometry Analyses, *Anal. Chem.*, 2020, **92**, 12750–12762.
24 S. Hammerum and C. B. Nielsen, Intramolecular hydrogen bonding and hydrogen atom abstraction in gas-phase aliphatic amine radical cations, *J. Phys. Chem. A*, 2005, **109**, 12046–12053.
25 I. Janovsky, W. Knolle, S. Naumov and F. Williams, EPR studies of amine radical cations, part 1: Thermal and photoinduced rearrangements of n-alkylamine radical cations to their distonic forms in low-temperature freon matrices, *Chem. – Eur. J.*, 2004, **10**, 5524–5534.
26 G. Sozzi, J.-P. Denhez, H. E. Audier, T. Vulpius and S. Hammerum, Intramolecular hydrogen atom abstraction with an eight-membered cyclic transition state in open-chain aliphatic aminium radicals, *Tetrahedron Lett.*, 1985, **26**, 3407–3408.
27 T. Bjoernholm, S. Hammerum and D. Kuck, Distonic ions as reacting species, *J. Am. Chem. Soc.*, 2002, **110**, 3862–3869.
28 K. Clarke, R. Edge, V. Johnson, E. J. Land, S. Navaratnam and T. G. Truscott, Direct observation of NH_2* reactions with oxygen, amino acids, and melanins, *J. Phys. Chem. A*, 2008, **112**, 1234–1237.
29 M. T. Schümperli, C. Hammond and I. Hermans, Reactivity of α-amino-peroxyl radicals and consequences for amine oxidation chemistry, *Phys. Chem. Chem. Phys.*, 2012, **14**, 11002–11007.
30 F. B. Jariwala, J. A. Hibbs, C. S. Weisbecker, J. Ressler, R. L. Khade, Y. Zhang and A. B. Attygalle, A distonic radical-ion for detection of traces of adventitious molecular oxygen (O_2) in collision gases used in tandem mass spectrometers, *J. Am. Soc. Mass Spectrom.*, 2014, **25**, 1670–1673.
31 B. B. Kirk, D. G. Harman, H. I. Kenttamaa, A. J. Trevitt and S. J. Blanksby, Isolation and characterization of charge-tagged phenylperoxyl radicals in the gas phase: direct evidence for products and pathways in low temperature benzene oxidation, *Phys. Chem. Chem. Phys.*, 2012, **14**, 16719–16730.
32 M. B. Prendergast, P. A. Cooper, B. B. Kirk, G. da Silva, S. J. Blanksby and A. J. Trevitt, Hydroxyl radical formation in the gas phase oxidation of distonic 2-methylphenyl radical cations, *Phys. Chem. Chem. Phys.*, 2013, **15**, 20577–20584.
33 O. J. Shiels, S. C. Brydon, B. L. J. Poad, D. L. Marshall, S. D. Houston, H. Xing, P. V. Bernhardt, G. P. Savage, C. M. Williams, D. G. Harman, B. B. Kirk, G. da Silva, S. J. Blanksby and A. J. Trevitt, Electrostatically tuning radical addition and atom abstraction reactions with distonic radical ions, *Chem. Sci.*, 2025, **16**, 2861–2878.
34 P. Ortega, S. Gil-Guerrero, L. Gonzalez-Sanchez, C. Sanz-Sanz and P. G. Jambrina, Spin-Forbidden Addition of Molecular Oxygen to Stable Enol Intermediates-Decarboxylation of 2-Methyl-1-tetralone-2-carboxylic Acid, *Int. J. Mol. Sci.*, 2023, **24**, 7424.
35 J. N. Harvey, Understanding the kinetics of spin-forbidden chemical reactions, *Phys. Chem. Chem. Phys.*, 2007, **9**, 331–343.
36 G. Bouchoux, J. Y. Salpin and D. Leblanc, A relationship between the kinetics and thermochemistry of proton transfer reactions in the gas phase, *Int. J. Mass Spectrom. Ion Processes*, 1996, **153**, 37–48.
37 E. P. L. Hunter and S. G. Lias, Evaluated gas phase basicities and proton affinities of molecules: An update, *J. Phys. Chem. Ref. Data*, 1998, **27**, 413–656.
38 P. J. Linstrom and W. G. Mallard, *NIST Chemistry WebBook, NIST Standard Reference Database Number 69*, National Institute of Standards and Technology, Gaithersburg MD, 2025.
39 K. Sovová, K. Dryahina and P. Španěl, Selected ion flow tube (SIFT) studies of the reactions of H_3O^+, NO^+ and O^{2+} with six volatile phytogenic esters, *Int. J. Mass Spectrom.*, 2011, **300**, 31–38.
40 D. Smith and N. G. Adams, The Selected Ion Flow Tube (Sift): Studies of Ion-Neutral Reactions, *Adv. At. Mol. Phys.*, 1988, **24**, 1–49.
41 T. Su and W. J. Chesnavich, Parametrization of the ion–polar molecule collision rate constant by trajectory calculations, *J. Chem. Phys.*, 1982, **76**, 5183–5185.
42 F. Neese, Software Update: The ORCA Program System-Version 6.0, *Wiley Interdiscip. Rev.: Comput. Mol. Sci.*, 2025, **15**, e70019.
43 F. Neese, An improvement of the resolution of the identity approximation for the formation of the Coulomb matrix, *J. Comput. Chem.*, 2003, **24**, 1740–1747.

44 F. Neese, F. Wennmohs, A. Hansen and U. Becker, Efficient, approximate and parallel Hartree-Fock and hybrid DFT calculations. A 'chain-of-spheres' algorithm for the Hartree-Fock exchange, *Chem. Phys.*, 2009, **356**, 98–109.
45 M. D. Hanwell, D. E. Curtis, D. C. Lonie, T. Vandermeersch, E. Zurek and G. R. Hutchison, Avogadro: an advanced semantic chemical editor, visualization, and analysis platform, *J. Cheminf.*, 2012, **4**, 17.
46 E. Caldeweyher, J. M. Mewes, S. Ehlert and S. Grimme, Extension and evaluation of the D4 London-dispersion model for periodic systems, *Phys. Chem. Chem. Phys.*, 2020, **22**, 8499–8512.
47 L. Wittmann, I. Gordiy, M. Friede, B. Helmich-Paris, S. Grimme, A. Hansen and M. Bursch, Extension of the D3 and D4 London dispersion corrections to the full actinides series, *Phys. Chem. Chem. Phys.*, 2024, **26**, 21379–21394.
48 E. Caldeweyher, C. Bannwarth and S. Grimme, Extension of the D3 dispersion coefficient model, *J. Chem. Phys.*, 2017, **147**, 034112.
49 R. Flammang, M. Barbieux-Flammang, E. Gualano, P. Gerbaux, H. T. Le, M. T. Nguyen, F. Turecek and S. Vivekananda, Ionized Benzonitrile and Its Distonic Isomers in the Gas Phase, *J. Phys. Chem. A*, 2001, **105**, 8579–8587.
50 D. M. Tomazela, A. A. Sabino, R. Sparrapan, F. C. Gozzo and M. N. Eberlin, Distonoid ions, *J. Am. Soc. Mass Spectrom.*, 2006, **17**, 1014–1022.
51 P. Pracht, F. Bohle and S. Grimme, Automated exploration of the low-energy chemical space with fast quantum chemical methods, *Phys. Chem. Chem. Phys.*, 2020, **22**, 7169–7192.
52 J. W. Ochterski, *Thermochemistry in Gaussian*, Gaussian, Inc., Pittsburg, PA, 2000.
53 C. Schaefer, K. Dryahina, P. Španěl, M. J. Perkins and V. S. Langford, *Data on 'SIFT-MS Analysis of Amines: Unusually efficient O2 Addition to the Radical Cation Product'*, National Data Repository, 2025, DOI: 10.48700/datst.zkt15-an280.
54 K. Watanabe and J. R. Mottl, Ionization Potentials of Ammonia and Some Amines, *J. Chem. Phys.*, 1957, **26**, 1773–1774.
55 P. Španěl and D. Smith, Selected ion flow tube studies of the reactions of H_3O^+, NO^+ and O^{2+} with several amines and some other nitrogen-containing molecules, *Int. J. Mass Spectrom.*, 1998, **176**, 203–211.
56 G. Pugliese, P. Trefz, B. Brock, J. K. Schubert and W. Miekisch, Extending PTR based breath analysis to real-time monitoring of reactive volatile organic compounds, *Analyst*, 2019, **144**, 7359–7367.
57 A. Spesyvyi, K. Sovova, D. Smith and P. Španěl, Increase of the Charge Transfer Rate Coefficients for NO(+) and O(2)(+ *) Reactions with Isoprene Molecules at Elevated Interaction Energies, *J. Phys. Chem. A*, 2018, **122**, 9733–9737.
58 N. G. Adams and D. Smith, The selected ion flow tube (SIFT); A technique for studying ion-neutral reactions, *Int. J. Mass Spectrom. Ion Phys.*, 1976, **21**, 349–359.
59 S. Hammerum, Rearrangement and hydrogen abstraction reactions of amine cation radicals: a gas-phase analogy to the Hofmann-Löffler-Freytag reaction, *Tetrahedron Lett.*, 1981, **22**, 157–160.
60 O. J. Shiels, P. D. Kelly, C. C. Bright, B. L. J. Poad, S. J. Blanksby, G. da Silva and A. J. Trevitt, Reactivity Trends in the Gas-Phase Addition of Acetylene to the N-Protonated Aryl Radical Cations of Pyridine, Aniline, and Benzonitrile, *J. Am. Soc. Mass Spectrom.*, 2021, **32**, 537–547.
61 B. F. Yates and L. Radom, Intramolecular hydrogen migration in ionized amines: a theoretical study of the gas-phase analogs of the Hofmann-Loeffler and related rearrangements, *J. Am. Chem. Soc.*, 1987, **109**, 2910–2915.
62 A. Haack, C. Ieritano and W. S. Hopkins, MobCal-MPI 2.0: an accurate and parallelized package for calculating field-dependent collision cross sections and ion mobilities, *Analyst*, 2023, **148**, 3257–3273.
63 V. Shrivastav, M. Nahin, C. J. Hogan and C. Larriba-Andaluz, Benchmark Comparison for a Multi-Processing Ion Mobility Calculator in the Free Molecular Regime, *J. Am. Soc. Mass Spectrom.*, 2017, **28**, 1540–1551.
64 M. O. Gnioua, P. Španěl and A. Spesyvyi, Gas-phase ion mobility of protonated aldehydes in helium measured using a selected ion flow-drift tube, *Rapid Commun. Mass Spectrom.*, 2024, **38**, e9767.
65 A. Spesyvyi, K. Sovová and P. Španěl, In-tube collision-induced dissociation for selected ion flow-drift tube mass spectrometry, SIFDT-MS: a case study of NO(+) reactions with isomeric monoterpenes, *Rapid Commun. Mass Spectrom.*, 2016, **30**, 2009–2016.